Thermography of Whole Blood during Laser Heating through Bare Fiber

Natalia Yu. Ignatieva[1], Olga L. Zakharkina[2], and Alexander P. Sviridov[2*]

[1] Faculty of Chemistry, Lomonosov Moscow State University, GSP-1, Leninskie Gory 1, building 3, Moscow 119991, Russia

[2] Institute of Photon Technologies of Federal Scientific Research Centre "Crystallography and Photonics" of Russian Academy of Sciences, 2 Pionerskayaya str., Troitsk 108840, Moscow, Russia

*** e-mail:** sviridoa@gmail.com

Abstract. The dynamics of temperature fields in whole blood during the action of continuous-wave (CW) laser radiation with wavelengths of 0.97, 1.56, and 1.68 μm for the temperature range up to 600 °C were studied. On the blood heating thermograms four characteristic stages differing in the heating rate were distinguished. Comparison of the obtained thermograms with the data of differential scanning calorimetry of blood and its thermogravimetry with mass spectrometry of released gases made it possible to attribute these stages as the temperature rises to protein denaturation and aggregation of blood cells, formation of coagulates, and carbonization of organic blood components coagulate and burning carbon. It has been established that the duration of separate stages of laser blood heating is determined mainly by the wavelength and power of laser radiation. The results obtained may be useful for the development of automated laser systems for the obliteration of varicose veins and other vascular tissues.

Keywords: IR laser heating; blood; IR thermography; coagulate; laser obliteration.

Paper #3542 received 10 Oct 2022; revised manuscript received 6 Dec 2022; accepted for publication 7 Dec 2022; published online 27 Dec 2022. doi: 10.18287/JBPE22.08.040513.

1 Introduction

Local laser heating of blood and vascular tissues, causing their ablation or coagulation, is currently widely used in medical practice to treat a number of diseases, stop bleeding during surgical operations [1–3]. Endovenous laser ablation (EVLA) [4] is widely used for minimally invasive treatment of varicose veins. This method is based on the delivery of laser radiation into the blood vessel through an optical fiber. The efficacy and safety for laser obliteration is largely ensured by an adequate choice of laser radiation settings, such as wavelength, power, optical fiber movement speed. These characteristics of laser exposure affect the rate of physical and chemical processes in the blood and vascular tissues that accompany laser heating. First of all, they include protein denaturation, aggregation of blood cells, and coagulation [1–4]. The formation of coagulate is the most important factor influencing the result of laser exposure to blood. As the temperature rises, the formation of vapor-gas bubbles [5], decomposition and oxidation of the organic components of biological tissues, and carbonization are observed [6–8]. A review of mechanisms and modeling outcomes under endovenous laser treatment is presented in Ref. [7]. As for computational models of EVLA, its use analytical solution of the transport equation of light propagation in an absorbing and scattering medium [9] and the equation, which is in fact transient heat conduction, with a source term equal to the absorbed volumetric power [7–10]. The absorption and scattering coefficients either do not change [7] or are directly related to carbon content. In the latter case, the temperature distribution resulting from heat conduction from the fiber tip was calculated by thermal finite element-modeling [10]. Optical-thermal response of laser-irradiated blood and vein walls can significantly increase the effective absorption coefficient, which creates conditions for positive

feedback and rapid overheating of a significant amount of adjacent tissues [7, 8].

It should be noted that near the tip of the optical fiber, the power density of laser radiation is usually maximum, and it is here that extreme conditions are reached in the first place [7, 8]. They are quite acceptable, and in many cases even necessary to ensure the correct mode of heating the vessel walls, provided that the overheated area is localized, and its dimensions, tissue changes and instruments are under automated control. Otherwise, complications are very likely [11]. This is largely due to the lack of detailed studies of the dynamic behavior of temperature fields during laser blood heating in a wide temperature range and the correlation of changes occurring in the blood with a specific temperature. Among the few works devoted to this problem, the work [12] should be noted. The authors of work [12], comparing the data of optical coherence tomography, measurements of surface temperature, and light transmission, obtained a lower temperature threshold of 110 °C for coagulate formation under laser irradiation with a wavelength of 532 nm and a pulse duration of 10 ms. Further studies are mainly devoted to comparing changes in the optical property under laser irradiation with temperature changes simulated using the thermal finite element-modeling [13, 14]. These comparisons showed that a cardinal change in the optical properties occurs at a calculated temperature of 80–95 °C, which gave grounds to conclude that photothermal coagulation began in this temperature range and the assumption of two stages of this process, taking into account the fact that the optical properties of blood are a complex function its composition and state of cells [14–16].

The purpose of this work is to establish the physicochemical processes occurring in whole blood during continuous laser heating through a bare fiber. During laser treatment at wavelengths of 0.97, 1.56, and 1.68 μm of whole blood, the dynamics of temperature fields was recorded. Laser wavelengths and power are in the range used in the EVLA procedure. The absorption coefficients of blood at these wavelengths differ significantly [17]. Physicochemical processes that occur with temperature variations were identified under calorimetry conditions with simultaneous analysis of thermal effects (differential scanning calorimetry), mass loss (thermogravimetry method) and mass spectrometric analysis of released gases. Comparison of the results of temperature changes and calorimetry made it possible to suggest a sequence of laser-induced changes in the blood. The results obtained may be useful for the development of automated laser systems for EVLC procedure.

2 Materials and Methods

Human blood samples were obtained from healthy volunteers. Heparinized whole blood was stored at 4 °C and used not longer than for 24 h. For calorimetric study red blood cells (RBCs) and plasma were separated by centrifugation for 15 min at 4000×g at 4 °C.

A plastic cylindrical cuvette with an inner diameter of 18 mm and a height of 10 mm was used for local laser blood heating. A hole 1 mm in diameter was made in the wall at a distance of 3 mm from the bottom of the cuvette. A bare optical quartz fiber with a core diameter of 0.6 mm and numerical aperture 0.22 was hermetically introduced through the hole, remaining horizontally oriented The fiber entered the hole at a distance of 3–4 mm, and the fiber tip was at a distance of at least 14 mm from diametrically opposite cuvette wall. The cuvette was filled with whole blood through a pipette dispenser so that the blood only merely covered the fiber.

A diode laser which emits a wavelength (λ) of 0.97 μm, an erbium-doped fiber laser (λ = 1.56 μm) and a fiber Raman laser (λ = 1.68 μm) were used in the experiments. All lasers were produced by IRE-Polus, Russia. The laser radiation was emitted in CW mode that is typical for EVLA procedure. The radiation power P was controlled by a power meter UP12-H (Gentec Electro-Optics, USA) and varied from 4 to 6 W in steps of 0.5 W for 1.56 μm and 1.68 μm lasers and from 9 to 11 W for 0.97 μm laser.

The space temperature distribution in the near-surface layer of blood under laser heating was monitored by means of a Model FLIRA655sc infrared camera operating with 100 Hz frame rate and equipped with a Model FOL25 objective lens. The camera was calibrated with a precise mercury thermometer by measuring the temperature of water heated in an open vessel up to 70 °C. The temperature was recorded with an accuracy of ±1 °C and a linear spatial resolution 0.08 mm. Measurements with infrared camera from outside through a thin glass plate (~100 μm) showed that the temperature field induced in the blood near the tip of optical fiber is almost uniform over the entire cross section of the fiber. So we assume that the difference between temperature measured near the blood surface and temperature at the axis of optical fiber is rather negligible. The example of the temperature field caused by laser radiation and recorded by the infrared scanner is depicted on the Fig. 1. The thermograms were processed using the FLIR Research IR Max software and the dynamics of the maximum temperature and the spatial distribution of temperature at selected time points were determined. For each pair of parameters λ, P measurements were repeated three times with the change of blood in the cuvette. Moreover, the fiber tip was cut after each applying. The scheme of the experimental setup is presented in the Fig.1.

The thermal behavior of blood was determined by simultaneous differential scanning calorimetry (DSC) and thermogravimetry (TGA) on-line coupled with a quadrupole mass spectrometer (QMS). Blood was heated in an open crucible placed in a Netzsch STA 449 C Jupiter thermal analyzer (Netzsch, Germany) under argon and air flow (80 ml/min) from 40 to 590 °C at a rate of 10 K/min. The QMS 403 C Aëolos Quadro unit was used to monitor and record the evacuated gas phase. Mass Spectrometry (MS) analysis was performed in a mode that allowed to set selected ion monitoring for the mass-to-charge ratios (m/z) from 10 to 100. The peaks corresponding to m/z = 18 is a

qualitative reflection of the appearance of water (H_2O) in the gas phase. The charge m/z = 30 indicates NO and m/z = 44 refer to processes leading to decomposition with complete combustion to CO_2.

Low-temperature transformations of components in blood, plasma, and centrifugate containing blood cells were determined by heating the materials in sealed crucibles placed in the furnace of a Phoenix DSC 204 differential scanning calorimeter (Netzsch, Germany). The initial and final temperatures were 25 and 90 °C, respectively, and the heating rate was 10 K/min.

3 Results and Discussion

The example of processed thermograms induced on blood surface under laser heating of blood is shown on Fig. 1. The space- and time- dependencies of the temperature fields looked rather similar for all laser wavelength we used. After the laser was turned on, an isothermal region with a linear size of 240 μm and a temperature along the boundary from 82 to 88 °C appeared in no more than 0.1 s (Fig. 2a). We considered the area to be isothermal when the temperature at the center and at the boundary differed by no more than 3–5 °C. These values are about the same for all wavelengths (82–88 °C).

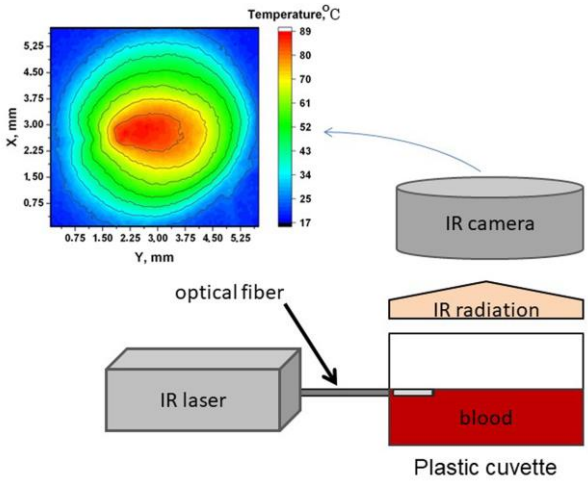

Fig. 1 Schematic representation of the experimental setup and the temperature field induced by laser radiation (temperature on the Celsius scale is on the right side).

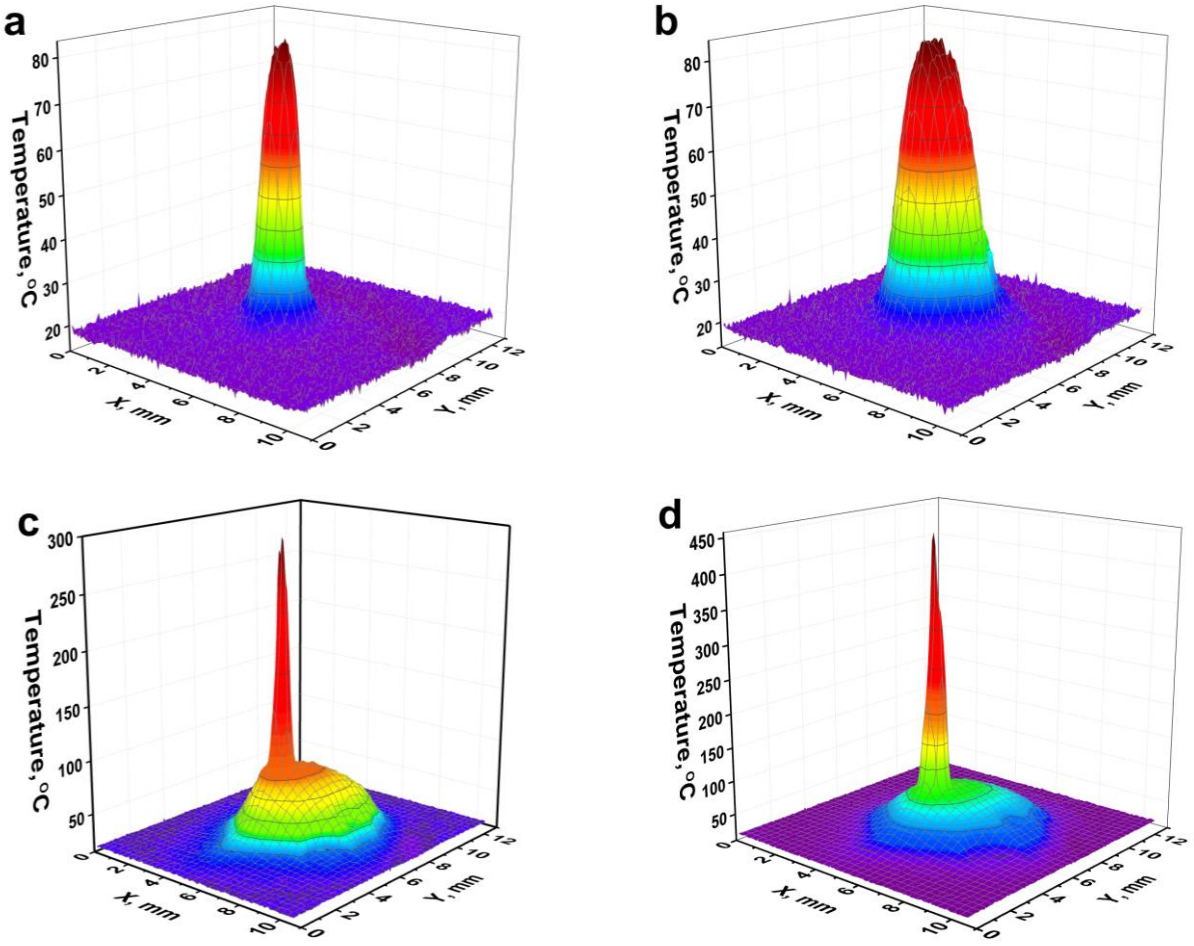

Fig. 2 The temperature distribution in the near-surface layer of blood under laser exposure (λ = 1.56 μm, P = 4.5 W) at critical moments: the start of the isothermal stage (a), the end of the isothermal stage (b), the rise of the maximum temperature (c), start of carbon burning (d).

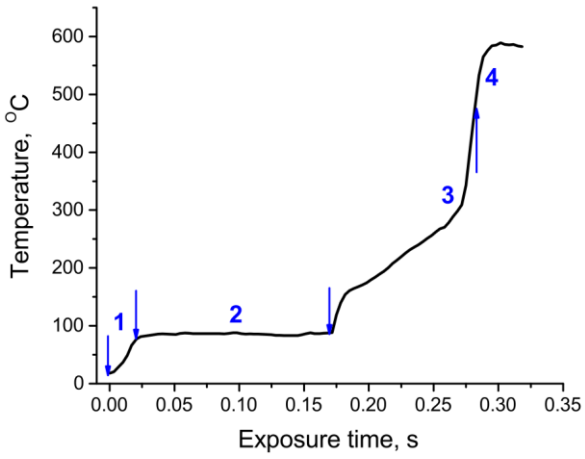

Fig. 3 Typical dynamics of the maximum temperature during blood heating by laser radiation (the example refers to the laser setting of λ = 0.97 μm and P = 10 W. Stages 1–4 are marked.

Further, the isothermal region expanded (Fig. 2b) and a hot pixel (~80 μm) appeared near its center, in which the temperature began to rise. We called the temperature at this point the maximum temperature T_m. The dynamics of T_m is shown in Fig. 3. The maximum temperature increased to 82 ± 2 °C (stage 1), and it kept this value during the time τ (stage 2). Then, a fairly sharp rise in temperature to 200 °C began (the first part of stage 3). This growth became slower in the second part of stage 3, lasting up to 280–330 °C (Fig. 2c). At stage 4, the heating rate increased sharply and reached 600 °C and higher in 0.01–0.04 s (Fig. 2d).

For a certain radiation power, which we called critical power P_{cr}, it was noted

- reduction of the isothermal stage to 0.01–0.04 s;
- degeneration of the isothermal plateau of stage 2 to an inflection point;
- nonresolving of the stage 3 and stage 4. The value of P_{cr} depended on the radiation wavelength. At powers above P_{cr}, individual heating stages were not determined. At powers below P_{cr}, the shape of the $T_m(t)$ curve was practically independent of P and λ.

On the other hand, the duration of the isothermal stage 2 (τ), coinciding with the time of existence of the isothermal region, depended on both λ and P. The lengths of the isothermal region along and across the direction of radiation at the end of stage 2, determined by the laser exposure time τ, are given in Table 1 for all λ and P used in experiments.

Table1 The duration of the isothermal stage 2 (τ) and lengths of the isothermal area*.

λ, μm	P, W	τ, s	The length along the fiber axis, mm	The length across the fiber axis, mm
0.97	9	0.78 ± 0.12	3.40 ± 0.25	2.20 ± 0.20
0.97	10	0.15 ± 0.03	2.50 ± 0.15	1.80 ± 0.15
0.97	11	0.02	1.62 ± 0.10	1.32 ± 0.12
1.56	4	0.61 ± 0.10	2.82 ± 0.20	2.42 ± 0.20
1.56	4.5	0.52 ± 0.06	2.05 ± 0.16	1.71 ± 0.15
1.56	5	0.02	0.37 ± 0.08	0.36 ± 0.08
1.68	4.5	1.5 ± 0.2	2.25 ± 0.21	1.70 ± 0.16
1.68	5	0.64 ± 0.10	1.81 ± 0.12	1.40 ± 0.15
1.68	5.5	0.16 ± 0.08	0.88±0.10	0.77±0.12
1.68	6	0.03 ± 0.01	0.46±0.08	0.46±0.08

* All values represent mean ± SD.

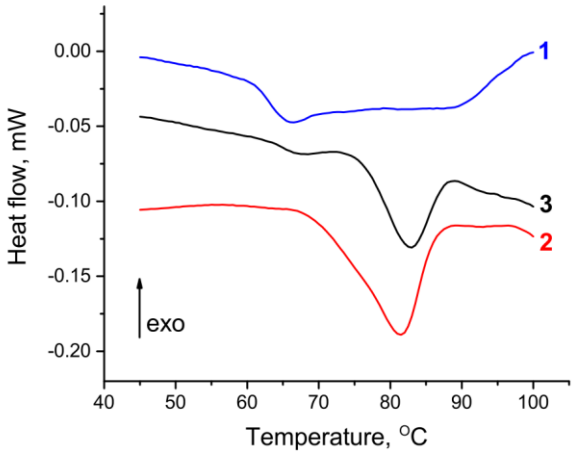

Fig. 4 DSC curves of plasma (1), RBCs (2) and whole blood (3) when heated to 100 °C.

DSC curves, obtained under plasma, RBCs and whole blood heating from 20 to 100 °C in closed crucibles are shown in Fig. 4. Comparative analysis of DSC curves makes it possible to identify some processes, occurring in whole blood when heated. So, at temperatures of 63–70 °C, denaturation of plasma proteins (albumin, immunoglobulin and fibrinogen) occurs, which is accompanied by heat absorption $\Delta H = 4$ J/g dry weight. An endothermic transition with a peak maximum of 81–83 °C and $\Delta H = 37$ J/g of dry weight is associated with hemoglobin denaturation and the breaking of multiple hydrogen bonds that stabilize macromolecules structure in RBCs [6, 18]. Obviously, damage to both the supramolecular integral structure and the native conformation and separate blood components leads to coagulation.

The results of simultaneous TGA-DSC-MS measurements of whole blood in air atmosphere are shown in Fig. 5a (TGA-DSC) and Fig. 5b (MS – formation of ionic fragments of H_2O, NO and CO_2). A mutual analysis of the TGA, DSC, and MS curves made it possible to establish the following stages of thermal destruction of blood in the temperature range of 60 to 600 °C:

– evaporation of water, a mass loss of 67% (60–130 ºC);
– decomposition of organic compounds starting as decarboxylation with release of CO_2) and oxidative deamination with release of NO and leading to carbonization, a mass loss of 42% of dehydrated residue and heat absorption (200–460 ºC);
– burning of carbonized residue, fast release of heat and CO_2, a mass loss of 30% of dehydrated residue (above 460 ºC). Note that in an argon atmosphere, the first two processes occur in the same temperature ranges, but there is no combustion.

Obviously, the detected temperature stages of laser blood heating (Fig. 3) can be associated with the physicochemical processes occurring during blood calorimetry. For a more accurate specification of the processes, the data of calorimetric measurements should be analyzed in combination with data on changes in the optical properties of blood under traditional [18], laser [14, 15] heating and low shear stress [19]. At stage 1 of heating, the transition of erythrocytes from a disc-shaped biconcave shape to a spherical one occurs, protein denaturation, cell aggregation and rupture of cell membranes [14, 15, 17, 18]. These processes determine the increase in light transmission [18].

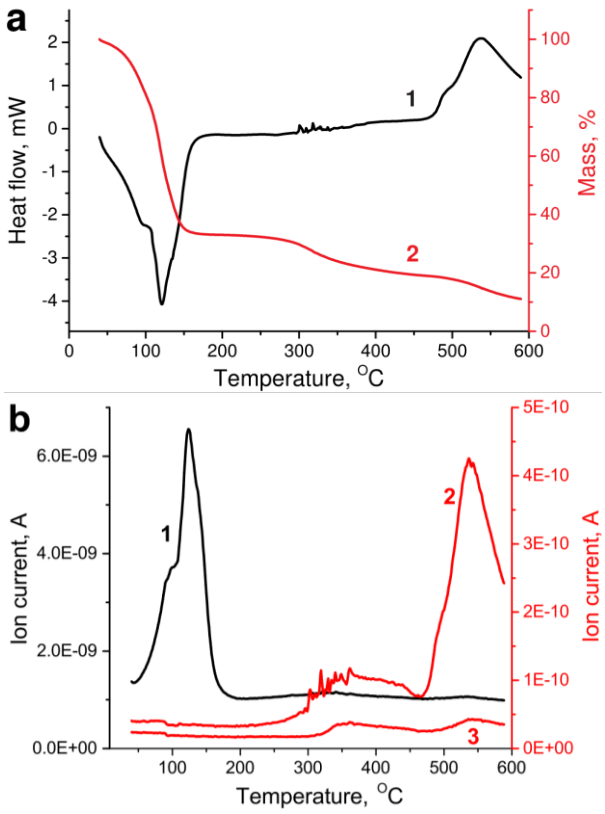

Fig. 5 Simultaneous TGA-DSC-MS analysis. (a) TG (2) and DSC (1) curves; (b) ion current associated with m/z = 18, H_2O (1), and m/z = 44, CO_2 (2) and m/z = 30, NO (3).

Recent studies [19] showed that aggregation leads to an increase in forward-scattered light intensity and decrease in back-scattered light intensity. Such changes in the scattering pattern indicate an increase in the anisotropy factor g. As a consequence, the effective absorption coefficient μ_{eff} decreases. Together, the decrease in radiation absorption, the consumption of absorbed energy for denaturation and heat dissipation make it possible to explain the existence of an isothermal region during laser exposure at stage 2. As the isothermal region expands, the processes of denaturation and aggregation proceed in an increasing volume of blood. In this case, the temperature gradient decreases (Fig. 2) and, consequently, the heat flux from the absorption region to the periphery decreases. The temperature rises in the zone of maximum absorption, where the actual coagulate is formed (the second phase of coagulation in the terminology of Ref. [14]). The heated-blood sample is becoming more opaque and transmission of light is reduced very quickly [14, 15, 17]. The formation of a coagulate marks the end of stage 2 and the beginning

of stage 3. The light absorption in the coagulate increases compared to the original blood [14, 15], its temperature increases already at the beginning of stage 3. After 200 °C, the decomposition of organic molecules begins with the absorption of heat. Perhaps it is this absorption of heat that leads to the fact that at the beginning of stage 3 the temperature rise slows down. By the middle of stage 3, organic molecules are partially decomposed to carbon, and in the second part of stage 3, the carbonized residue absorbs most of the laser radiation and the temperature rises even faster. After evaporation of water from the blood layer, covering the fiber, at a temperature of about 450 °C, organic residues and carbon are oxidized to CO_2 and NO by air oxygen (Fig. 5). Oxidation is accompanied by the release of heat and a sharp jump in temperature up to 600 °C and above.

All processes described above occur when the blood is heated using laser radiation with a power of $P \le P_{cr}$. However, both the power and the wavelength of radiation determine the temporal and spatial characteristics of physicochemical processes. Thus, the following patterns are observed (Table 1):

- the lifetime of the isothermal region τ decreases with increasing radiation power for all λ. At $P > P_{cr}$ the isothermal stage is not fixed at the frame rate we use (100 Hz);
- the size of isothermal region at $P = P_{cr}$ and the moment $t = \tau$ in the wavelength series 0.97–1.68–1.56 μm decreases.

The first pattern can be associated with an increase in the heating rate, therefore, the rates of denaturation, aggregation and coagulation increase. The coagulate, characterized by a large absorption, is formed the faster, the greater the power. The decrease in τ and, consequently, the size of the isothermal region over time τ as P increase is comprehensible. Finally, at a certain power of laser radiation, the processes of denaturation-aggregation and coagulation will proceed so quickly that the monitoring of individual stages is impossible using our experimental equipment. Apparently, this occurs when the area of volumetric denaturation-aggregation-coagulation becomes smaller than the area of effective absorption of laser radiation, determined by the characteristic penetration depth $\delta=1/\mu_{eff}$. The values of μ_{eff} , calculated from the known absorption and scattering coefficients [20] according to the standard approach [3], are 5.1–12.6–19.4 cm^{-1}, and the value of δ reaches 2, 0.8, and 0.5 mm in the wavelength series 0.97–1.68–1.56 μm, 1.68–1.56 μm, respectively. Indeed, at critical power for each λ, the longitudinal dimensions of the isothermal region (Table 1) turn out to be less than characteristic penetration depth. The decrease in the size of the isothermal region at the moment $t = \tau$ at $P=P_{cr}$ decreases symbatically δ in the wavelengths sequence 0.97–1.68–1.56 μm.

Simulation the temporal temperature distributions using the thermal finite element-modeling can clarify the sequence of events occurring during laser blood heating at any power, including $P > P_{cr}$. However, for the correct modeling of these processes, the following factors must be taken into account:

- quantitative change in the effective absorption coefficient of radiation in the areas of denaturation-aggregation-coagulation and carbonization;
- heat effects of denaturation, decomposition of organic compounds and combustion.

It is also necessary to determine the temperature-time criterion for the formation of coagulate in the blood under laser heating. This significantly complicates the model, and the formation of ideas about the physicochemical processes on the basis of the obtained experimental data, in our opinion, turns out to be the most productive for practical application. So, in the EVLC procedure, the optical fiber moves in the blood vessel at a speed of 0.5–2 mm/s. Efficient heating of the vein wall is possible only with the rapid onset of stage 3 or the reduction of τ to a minimum. This is what happens at critical power. Note that the P_{cr} for wavelengths of 0.97–1.68–1.56 μm obtained in this study coincide with the critical powers obtained experimentally for the effective destruction of the varicose vein wall [21, 22].

4 Conclusions

The data of IR thermography of blood subjected to IR laser radiation were compared with the data of thermal and thermogravimetric analysis. Based on the combined results, a sequence of physicochemical processes occurring during IR laser heating is proposed. Changes in the blood include proteins denaturation and cells aggregation, coagulate formation, carbonization of the organic compounds, and their combustion. The characteristics of IR laser radiation (λ and P) determine the duration of the individual stages of the process. With an increase in power above the critical value, all stages proceed almost simultaneously in the region of effective absorption of laser radiation.

Lasers with light wavelengths of 1.56 and 1.68 μm give the same effect of coagulate formation and its carbonization at a lower power than laser with light wavelength of 0.97 μm. Due to this, the number of tissue perforations and other undesirable effects caused by tissue overheating under EVLA decreases essentially. Therefore, it is preferable to carry out the EVLA procedure by laser light, which effective absorption coefficient of blood is not less than about 10 cm^{-1}.

Disclosures

The authors have no relevant financial interest in this article and no conflict of interest to disclose.

Acknowledgements

This study was performed within the State assignment for the Federal Scientific Research Centre ‘Crystallography and Photonics’ of the Russian Academy of Sciences in part of laser technologies and State assignment No. AAAA-A21-121011990019-4.

References

1. S. L. Jacques, "Laser-tissue interactions. Photochemical, photothermal, and photomechanical," Surgical Clinics of North America 72(3), 531–558 (1992).
2. N. Katta, D. Santos, A. B. McElroy, A. D. Estrada, G. Das, M. Mohsin, M. Donovan, and T. E. Milner, "Laser coagulation and hemostasis of large diameter blood vessels: effect of shear stress and flow velocity," Scientific Reports12, 8375 (2022).
3. M. H. Niemz, Laser-Tissue Interactions Fundamentals and Applications, 3rd ed., Springer, Berlin (2007).
4. C.-M. Fan, R. Rox-Anderson, "Endovenous laser ablation: mechanism of action," Phlebology 23(5), 206–213 (2008).
5. V. M. Chudnovskii, V. I. Yusupov, O. L. Zakharkina, N. Yu. Ignatieva, V. S. Zhigarkov, M. N. Yashkin, and V. N. Bagratashvili, "Contribution of laser-induced gas-vapor-liquid dynamics to the mechanism of endovenous laser ablation," Modern Technologies in Medicine 8(2), 6–11 (2016).
6. C. G. Mothé, T. Carestiato, and M. B. Águila, "Thermoanalytical investigation of blood," Journal of Thermal Analysis and Calorimetry 85(2), 247–251 (2006).
7. W. S. Malskat, A. A. Poluektova, C. W. van der Geld, H. A. Neumann, R. A. Weiss, C. M. Bruijninckx, and M. J. van Gemert, "Endovenous laser ablation (EVLA): a review of mechanisms, modeling outcomes, and issues for debate", Lasers in Medical Sciences 29, 393–403 (2014).
8. R. R. van den Bos, M. A. Kockaert, H. A. M. Neumann, R. H. Bremmer, T. Nijsten, and M. J. C. van Gemert, "Heat conduction from the exceedingly hot fiber tip contributes to the endovenous laser ablation of varicose veins," Lasers in Medical Sciences 24(2), 247–251 (2009).
9. S. R. Mordon, B. Wassmer, and J. Zemmouri, "Mathematical modeling of 980-nm and 1320-nm endovenous laser treatment," Lasers in Surgery and Medicine 39(3), 256–265 (2007).
10. A. A. Poluektova, W. S. J. Malskat, M. J. C. van Gemert, M. E. Vuylsteke, C. M. A. Bruijninckx, H. A. M. Neumann, and C. W. M. van der Geld, "Some controversies in endovenous laser ablation of varicose veins addressed by optical–thermal mathematical modeling," Lasers in Medical Sciences 29(2), 441–452 (2014).
11. D. Dexter, L. Kabnick, T. Berland, G. Jacobowitz, P. Lamparello, T. Maldonado, F. Mussa, C. Rockman, M. Sadek, L. E.Giammaria, and M. Adelman, "Complications of endovenous lasers," Phlebology 27(Suppl 1), 40–45 (2012).
12. T. J. Prefer, B. Choi, G. Vargas, K. M. McNally, and A. J. Welch, "Mechanisms of laser-induced thermal coagulation of whole blood in vitro," Proceedings of SPIE 3590, 20–31 (1999).
13. J. K. Barton, D. P. Popok, and J. F. Black, "Thermal analysis of blood undergoing laser photocoagulation," IEEE Journal of Selected Topics in Quantum Electronics 7(6), 936–943 (2001).
14. J. F. Black, N. Wade, and J. K. Barton "Mechanistic comparison of blood undergoing laser photocoagulation at 532 and 1,064 nm," Lasers in Surgery and Medicine 36(2), 155–165 (2005).
15. M. Takahashi, A. Ito, Sh. Miyoshi, T. Kimura, S. Takatsuki, K. Fukumoto, K. Fukuda, and T. Arai, "Study of blood charring precursor states using backscattering at 663 nm from blood and optical window boundary," Lasers in Surgery and Medicine 44, 508–513 (2012).
16. V. V. Tuchin (Ed.), Handbook of Optical Biomedical Diagnostics, 2nd ed., SPIE, Bellingham, Washington, USA (2016).
17. N. C. Garbett, J. J. Miller, A. B. Jenson, and J. B. Chaires, "Calorimetry outside the box: a new window into the plasma proteome," Biophysical Journal 94, 1377–1383 (2008).
18. S. Mordon, Ph. Rochon, G. Dhelin, and J. C. Lesage, "Dynamics of temperature dependent modifications of blood in the near-infrared," Lasers in Surgery and Medicine 37(4), 301–307 (2005).
19. A. Semenov, A. Lugovtsov, P. Ermolinskiy, K. Lee, and A. Priezzhev, "Problems of red blood cell aggregation and deformation assessed by laser tweezers, diffuse light scattering and laser diffractometry," Photonics 9, 238 (2022).
20. N. Bosschaart, G. J. Edelman, M. C. G. Aalders, T. G. van Leeuwen, and D. J. Faber, "A literature review and novel theoretical approach on the optical properties of whole blood," Lasers in Medical Sciences 29(2), 453–479 (2014).
21. N. Yu. Ignat'eva, O. L. Zakharkina, A. P. Sviridov, K. V. Mazaishvili, and A. B. Shekhter, "Estimation of a minimum laser power with wavelengths of 1.47, 1.56, and 1.68 mm for efficient obliteration of varicose veins," Quantum Electronics 52(1), 78–82 (2022).
22. N. Ignatieva, O. Zakharkina, A. Kurkov, M. Molchanov, and K. Mazayshvili, "Analysis of the vein wall destruction under endovenous laser ablation in an ex vivo model," Journal of Cosmetic and Laser Therapy 23(7–8), 163–169 (2021).